PCCP

Accepted Manuscript

This is an *Accepted Manuscript*, which has been through the Royal Society of Chemistry peer review process and has been accepted for publication.

Accepted Manuscripts are published online shortly after acceptance, before technical editing, formatting and proof reading. Using this free service, authors can make their results available to the community, in citable form, before we publish the edited article. We will replace this *Accepted Manuscript* with the edited and formatted *Advance Article* as soon as it is available.

You can find more information about *Accepted Manuscripts* in the Information for Authors.

Please note that technical editing may introduce minor changes to the text and/or graphics, which may alter content. The journal's standard Terms & Conditions and the Ethical guidelines still apply. In no event shall the Royal Society of Chemistry be held responsible for any errors or omissions in this *Accepted Manuscript* or any consequences arising from the use of any information it contains.

ROYAL SOCIETY OF CHEMISTRY

www.rsc.org/pccp

Electronic Structure Engineering of Various Structural Phases of Phosphorene

Sumandeep Kaur[1*], Ashok Kumar[2*], Sunita Srivastava[1*] and K. Tankeshwar[3*]

[1]*Department of Physics, Panjab University, Chandigarh 160014, India*
[2]*Centre for Physical Sciences, School of Basic and Applied Sciences, Central University of Punjab, Bathinda, 151001, India*
[3]*Department of Physics, Guru Jambheshwar University of Science and Technology, Hisar, 125001, Haryana, India*

(May, 2016)

*Email:

Sumandeep Kaur (dusuman0015@gmail.com)

Ashok Kumar (ashok.1777@yahoo.com)

Sunita Srivastava (sunita@pu.ac.in)

K. Tankeshwar (tkumar@gjust.org)

Physical Chemistry Chemical Physics Accepted Manuscript

Abstract

We report tailoring in the electronic structure of various structural phases of phosphorene (α-P, β-P, γ-P and δ-P) based homo- and hetero-bilayers through in-plane mechanical strains, vertical pressure and transverse electric field by employing density functional theory. In-plane biaxial strains have considerably modified the electronic bandgap of both homo- and hetero-bilayers while vertical pressure induces metallization in the considered structures. γ-P homo-bilayer structure showed highest ultimate tensile strength (UTS ~ 6.21 GPa) on in-plane stretching. On the application of transverse electric field, the variation in bandgap of hetero-bilayers was found to be strongly dependent on the polarity of applied field which is attributed to the counterbalance between external electric field and internal field induced by different structural phases and heterogeneity in the arrangements of atoms of each surface of hetero-bilayer system. Our results demonstrate that electronic structure of considered hetero- and homo-bilayers of phosphorene could be modified by biaxial strain, pressure and electric field to achieve the desired properties for future nano-electronic devices.

Physical Chemistry Chemical Physics Accepted Manuscript

Physical Chemistry Chemical Physics Accepted Manuscript

1. Introduction

The exquisite electronic properties of graphene which include presence of massless Dirac fermions; high carrier mobility; excellent electrical and thermal conductivity, have won the noble prize 2010 for its discoverers [1]. However, the lack of bandgap in graphene limits its applications in nano and optoelectronics, which has therefore, triggered the interest of scientists in graphene-alternatives that currently lead to the emergence of a number of 2D materials such as silicene, germanene, hexagonal boron nitride (h-BN) and transition metal dichalcogenides (TMDs) [2-4]. Silicene and germanene are semi-metallic in nature similar to graphene, while hexagonal boron nitride is an insulator and TMDs are semiconductors [5-6].

Recently, layered phosphorous which is a new member of the family of 2D materials, have gathered a great deal of attention because of the possibility of mechanical exfoliation of layered bulk black phosphorous (BP) to yield few layer phosphorene [7] with a sizable bandgap of ~ 1 eV [8]. Note that the carrier mobility of phosphorene is ~ 1000 cm^2/V/s [9-10] which is considerably higher than a value ~ 200 cm^2/V/s obtained for 2D layered TMDs. Monolayer black phosphorene is also found to exhibit giant phononic anisotropy that can be tuned by strain and there is also an orientation dependent anisotropy in interlayer coupling of few-layer phosphorene [11]. The first principles calculations reveal that not only black phosphorene (α-P), but other phases such as blue-phospherene (β-P) [12], gamma-phosphorene (γ-P) [13] and delta-phosphorene (δ-P) [13-14] possess energetically and thermodynamically stable structures which require greater attention. A very recent study has predicted another four monolayer phosphorous allotropes with energetically stable structures i.e., ε-P, ζ-P, η-P and θ-P and through their hybridization another five energetically favorable structures can be formed [15]. Although, various methods like cleavage with tape, liquid-

phase exfoliation, plasma-assisted fabrication [16] and chemical vapor deposition [17] have been used to fabricate single or few layer black phosphorous (α-P) but the experimental realization of the other stable allotropes of phosphorene and their multilayer structure remain missing in the literature. Experimental results on van der Waals heterostructures have not been reported probably due to poor control in stacking the heterostructures. Thus, sincere and consecrated efforts are required from the experimentalists from materials and chemistry community to carry out experiments for fabricating heterostructures of various allotropes of phosphorene.

The possibility of band structure engineering by the formation of heterostructures based on 2D materials to develop novel devices opens up a new area of research [18-19]. The layered structures of various phases of phosphorene exhibit strong covalent bonding which holds the in-plane atoms, while the vertically stacked layers are held together by weak van der Waal forces. Due to the layered nature, phosphorene offers the opportunity to fabricate devices based on vertical heterostructures for novel nano- and opto-electronic applications *e.g.* h-BN/phosphorene heterostructure shows the possibility to assist experimentalists in identifying different structural phases of phosphorus [20]; phosphorene/graphene heterostructure shows ohmic as well as rectifying character [21] that make it as a potential electrode material in Li batteries [22]. Both h-BN as well as graphene are found to effectively protect the degradation of phosphorene while keeping its pristine electronic properties intact and they are also able to tune its carrier dynamics and optical properties [23]; phosphorene/MoS_2 acts as p-n diode [24] with very high photo detection power and CMOS inverter [25] with the possibility to be used as a novel channel material for future electronic applications; metal/BP interfaces such as Cu/BP forms ohmic contact while Zn/BP and In/BP form Schottkey contacts [26] in devices; etc.

Physical Chemistry Chemical Physics Accepted Manuscript

Furthermore, the electronic properties of nano materials including heterostructures can be modulated by applying external electric field, in-plain mechanical strains and vertical pressures which are considered to be novel and promising ways to modify the fundamental bandgap of the 2D materials [27-29]. For characterizing the inhomogeneous distribution of strain and its measurements, the strain-induced frequency shifts and variation in energy spacing between peaks of the characteristic vibrational mode in Raman spectra can be analyzed. R. Fei and L. Yang have used this method to quantify arbitrary strain distributions in monolayer black phosphorene [30]. Note that the tuning of fundamental direct bandgap of black phosphorous with number of layers, electric field and in-plane layer compression or expansion make few layer phosphorene as a promising candidate for many applications *e.g.* photodetector in visible to infrared light [31-32], novel thermoelectric material [33-34] with possible applications in portable electronic systems, gas sensor [35], in advanced battery application [36], etc.

Although black phosphorene (α-P) has already been studied in literature but less attention has been paid to the other three energetically and thermodynamically favorable structural phases *i.e.* β-P, γ-P and δ-P. Therefore, in the present paper, we have looked into the details of electronic properties of vertical heterostructures (homo- and hetero-bilayers) of the various structural phases of phosphorene by taking into consideration the effect of external electric field, in-plane strains and vertical pressure.

2. Computational Method

All the calculations have been performed by using SIESTA simulation package [37]. Norm-conserving Troullier Martin pseudo potential in fully separable Kleinman and Bylander form has been used to treat the electron-ion interactions [38]. The exchange and correlation energies have

Physical Chemistry Chemical Physics Accepted Manuscript

been treated within both GGA-PBE and van der Waals (vdW)-DRSLL functional [39]. The Kohn Sham orbitals were expanded as a linear combination of numerical pseudo atomic orbitals using a split-valence double zeta basis set with polarization functions (DZP). Throughout geometry optimization, the confinement energy of numerical pseudo-atomic orbitals is taken as 0.01 Ry. Minimization of energy was carried out using standard conjugate-gradient (CG) technique. Structures were relaxed until the forces on each atom were less than 0.01 eV/Å. Monkhorst-Pack scheme is used to sample Brillouin zone with a 10×10×1 mesh for the calculations based on hetero-bilayers and a 30×30×1 mesh for homo-bilayers. The spacing of the real space used to calculate the Hartree exchange and correlation contribution of the total energy and Hamiltonian was 450 Ry. A vacuum region of about 20 Å along perpendicular to 2D plane has been used in calculations to prevent the superficial interactions between the periodic images.

3. Results and Discussions

The two dimensional (2D) crystal structures of α-P, γ-P and δ-P have rectangular primitive cell with 4, 4 and 8 atoms respectively, while β-P possess 2 atoms in the hexagonal primitive cell [13]. All the considered phases of monolayer phosphorene *i.e.* α-P, β-P, γ-P and δ-P, are semiconductors with the calculated bandgap values 1.12 eV, 2.05 eV, 0.79 eV and 0.62 eV respectively. The bandgap values calculated using GGA-PBE functional are 0.94 eV, 2.02 eV, 0.55 eV and 0.29 eV respectively for α-P, β-P, γ-P and δ-P. Our VDW-DRSLL results are in better agreement with the experimental values obtained for α-P (1.45 eV) [25]. The valance band maximum (VBM) and conduction band minimum (CBM) in α-P and δ-P lies on the same high symmetry point making them direct bandgap semiconductors while β-P and γ-P are indirect bandgap semiconductors (Figure S1 of ESI). Note that the Brillouin zone of α-P, γ-P and δ-P are rectangular with high symmetry path

Physical Chemistry Chemical Physics Accepted Manuscript

S-Y-Γ-X-S while β-P possess hexagonal Brillouin zone with high symmetry path K-Γ-M-K. The states around the Fermi level for all the phases are mainly contributed by the p-orbitals of P atoms.

3.1. Homo-bilayers of phosphorene :

Similar to graphene, the bilayers of phosphorene can have two different types of stacking pattern i.e. AB and AA. The crystal structure of homo-bilayers (i.e. two layers with same structural phase) with primitive cell is shown in Figure 1. Homo-bilayers of α-P, β-P, γ-P and δ-P possess 8, 4, 8 and 16 atoms respectively in 1 x 1 supercells. Our total energy calculations reveal AB-stacking to be most favorable for α-P bilayer, while β-P (hexagonal unitcell), γ-P and δ-P bilayers prefer AA-stacking pattern. The difference in total energy between two different types of stacking in α-P, β-P, γ-P and δ-P bilayers is found to be 0.09 meV/atom, 0.02 meV/atom, 4 meV/atom and 2 meV/atom respectively. Note that previous first principles calculations of α-P also predict AB-stacking pattern to be most favorable [40]. In another report [41], AA-stacking marginally prefers over AB-stacking in β-P bilayers which is consistent with our prediction. Homo-bilayers of α-P show direct bandgap of 0.92 eV which is in good agreement with other reported values in literature [42] whereas β-P (hexagonal unitcell) is indirect bandgap semiconductor with bandgap value 1.49 eV (Figure 2 & Table 1). Our van der Waals functional based calculations indicate γ-P bilayer to be an indirect bandgap semiconductor with a bandgap value of 0.29 eV (Figure 2(c)) while our GGA-PBE calculations predict metallic character of γ-P (Figure S2(a) of ESI) as also reported in literature [13]. Using VDW-DRSLL functional, we find δ-P bilayer as a direct bandgap semiconductor with a bandgap value of 0.38 eV while our GGA-PBE calculations predict Dirac cone like character at the Fermi level of δ-P bilayer (Figure 2(d) and Figure S2(b) of ESI), which mainly consists of the 3p orbitals of P atoms. Note that four layer thick black phosphorene [43] and hydrogenated blue phosphorene [44] are also found to possess graphene-like Dirac cone features. However, it has been

Physical Chemistry Chemical Physics Accepted Manuscript

well-known that the GGA-PBE cannot accurately describe the vdW interaction and even for the case of mono and bilayer α-P, it is found to underestimate the bandgap [42]. So, for further calculations of van der Waals bilayers, we have used VDW-DRSLL functional that incorporates the vdW interactions.

Our calculated binding energy per atom of homo-bilayers is found to be of the order of a few meV (Table 1) which indicates weak van der Waals interactions between the layers. The binding energy (E_b) per atom was calculated as: $E_b = [E- (E_1+E_2)]/N$, where E_1 and E_2 are the total energy of isolated layers, E is the total energy of bilayer system and N is the total number of atoms in the supercell. In contrast to monolayer, the electronic band structure of bilayers show reduction in electronic bandgap which is attributed to the splitting of energy levels due to interlayer interactions (Figure S1 and Figure 2) [42]. In order to get further insight into the interlayer interactions, the charge density difference has been calculated which shows accumulation of charge between the layers (Figure S3 of ESI) that results into the reduction of bandgap in bilayers. Here the charge density difference profile is obtained as $\Delta\rho = \rho-(\rho_1+\rho_2)$, where ρ is charge density of bilayer while ρ_1, ρ_2 are charge densities of isolated monolayers.

3.2.Hetero-bilayers of phosphorene :

Now we consider the four possible commensurable vertical hetero-bilayer structures *i.e.* α-P/β-P, γ-P/δ-P, γ-P/β-P and δ-P/β-P (Figure 3) of four structural phases of phosphorene. The commensurable bilayer structures are constructed in order to minimize the interfacial strain between the layers of different phases. For example, the supercell of α-P/β-P (Figure 3(a)) consists of 5×1 unitcells of monolayer α-P vertically stacked over 4×1 unitcells of monolayer β-P, that results into ~ 2.2 % lattice mismatch between the vertically stacked layers. Similarly, the choice of 5×1/3×1

Physical Chemistry Chemical Physics Accepted Manuscript

unitcells in γ-P/δ-P (Figure 3(b)), 1×1/1×1 unitcells in γ-P/β-P (Figure 3(c)) and 3×1/5×1 unitcells of δ-P/β-P (Figure 3(d)), produce minimum lattice mismatch of about 2.7 % in γ-P/δ-P, 4.6 % in γ-P/β-P and 6.5 % in δ-P/β-P (Table 2). Note that bilayer α-P twisted by an angle 2.5^0 has been found to possess AA, AB and AC stacking regions within its Moire pattern [45]. Our bilayer systems particularly those with large lattice mismatch (γ-P/β-P and δ-P/β-P), may have the possibility of the formation of Moire pattern with different stacking regions and in that case the bandgaps would possibly be the lowest of different stacking styles.

Note that, in order to make heterostructure of β-P with other allotropes, its rectangular unit cell is used to obtain the commensurable lattice. We have calculated the lattice constant a = 3.41 Å and b = 5.91 Å for rectangular unit cell of β-P. The bandgap value 2.05 eV (Figure S1 of ESI) is in line with the value calculated with hexagonal unit cell. The favorable stacking pattern is AB in bilayer of β-P (rectangular unitcell), however the energy difference between the total energy of both the stacking patterns is negligibly small (0.5 meV/atom). Figure S4 and S5 of ESI shows the stacking pattern and the band structure of β-P in rectangular unit cell with a bandgap value of 1.46 eV.

The binding energy per atom in the considered hetero-bilayers structures is of the order of a few meV which indicates weak van der Waals interactions between the hetero-bilayers. It is interesting to note that the band structures of considered hetero-bilayers have indirect bandgap in nature except γ-P/δ-P which shows direct bandgap (Figure 4) while their monolayer counterparts i.e., α-P and δ-P have direct bandgaps and β-P and γ-P have indirect bandgaps (Figure S1). The calculated charge density difference profile (Figure S6 of ESI) show charge redistributions between the layers that result in a smaller energy gap in electronic structure.

3.3 Ultimate tensile strength of homo- and hetero-bilayers:

Physical Chemistry Chemical Physics Accepted Manuscript

To examine the in-plane flexibility or tensile strength of both homo- and hetero-bilayers, we have applied an in-plane stretching strains along x and y directions simultaneously. The mechanical strain, $e = \Delta a/a_0$, was applied in small steps where a_0 is the equilibrium lattice constant and Δa is the change in lattice constant obtained after deformation of the lattice [46]. The maximum stress that a bilayer system can withstand before breaking gives its ultimate tensile strength (UTS). The value of UTS is the point at which the slope of the strain-stress curve becomes zero. The strain-stress can be determined by calculating the stress tensor components in response of the strain tensor. The stress tensor is defined as a positive derivative of total energy with respect to the strain tensor [37].

On the application of biaxial strain, the stress obtained along x and y direction in all the considered structures is shown in Figure 5. The stress-strain curves for hetero-bilayers were obtained after subtracting the stress introduced due to lattice mismatch at zero strain value. The values of strain at which the ultimate tensile strength (UTS) is obtained for x and y direction and the UTS values are listed in Table 3. The highest UTS values among homo-bilayers are found for γ-P structural phase where the UTS values 6.21 GPa & 4.47 GPa along x and y direction respectively have been obtained with respective ultimate strain values 32 % and 22 %. Note that the UTS and ultimate strain value of β-P homo-bilayers in rectangular unit cell have been calculated as 4.84 GPa and 26 % along x as well as along y direction (Figure S7 of ESI). Similarly, highest UTS values among hetero-bilayers are obtained for γ-P/β-P (Table 3). We have found UTS values in the range of 2.8-6.2 GPa for considered homo- and hetero-bilayers. The differences in stress values along x and y directions may be attributed to the structural differences along the two directions or the differences in lattice constants along x and y directions.

3.4 Bandgap as a function of in-plan strain:

Physical Chemistry Chemical Physics Accepted Manuscript

Now we consider the effect of biaxial tensile strain on the bandgap of considered homo- and hetero-bilayers (Figure 6). The bandgap of homo-bilayer (in case of α-P, γ-P and δ-P) initially increases up to 6 % , 4 % and 8 % applied strain values respectively while on further increasing the strain the bandgap decreases to 0 eV at 34 %, 14 % and 34 % of strain respectively for α-P, γ-P and δ-P (Figure 6(a)). But strain values at which the metallization is obtained in α-P and δ-P are higher than their respective UTS values. In β-P homo-bilayer, the bandgap decreases with the application of strain with the occurrence of a semiconductor-to-metal transition at 16 % value of strain. Also, there occurs a direct to indirect bandgap transition at 4 % (4 %) and then indirect to direct bandgap transition at 23 % (26 %) of strain value in case of α-P (δ-P) bilayer. However, in case of β-P (γ-P) bilayer, the bandgap changes from indirect to direct at 8 % (2 %) of applied strain. In β-P bilayer there also occurs a direct to indirect bandgap transition at e = 10 %.

In all the considered hetero-bilayers, except γ-P/β-P, the bandgap first increases with the application of strain and then decreases and becomes less than 0.25 eV at 25 % of strain (Figure 6 (b)). A closer examination at the band structure of all the hetero-bilayers show that an initial increase in the bandgap with the application of strain is due to the simultaneous shift of VBM and CBM away from the Fermi level. Decrease in bandgap after attaining a maximum value is attributed to the simultaneous shift of VBM and CBM towards the Fermi level. As a representative case, the band structure of α-P/β-P at various values of in-plane biaxial strain is given in Figure S8 of ESI. The applied in-plan strain shift the VBM and CBM that leads to modification in band gap which is attributed to the redistribution of the out-of-plan atomic orbitals. In γ-P/β-P bilayer, however, application of strain shifts the VBM and CBM towards the Fermi level until the bandgap reduces down to zero, producing metallization at 18 % strain value. We have also found indirect-to-direct

Physical Chemistry Chemical Physics Accepted Manuscript

bandgap transition at 6 % (10 %) (10 %) and then direct-to-indirect gap transition at 20 % (16 %) (18 %) in α-P/β-P (γ-P/β-P) (δ-P/β-P) bilayers.

3.5 Effect of Vertical Pressure:

In order to see the effect of applied normal compression strain (e_z), we define it as $e_z = (R_0 – R)/R_0$, where R is the interlayer distance and R_0 is the equilibrium value of interlayer distance. We decrease the interlayer distance of the bilayers, starting from the equilibrium value, in steps of 0.1 Å and calculate the corresponding normal compression strain (NCS) and bandgap. Figure 7 shows the variation of bandgap with (NCS) for all the considered systems. α-P, γ-P and δ-P bilayers show negligible change in bandgap up to e_z = 20 %, 10 % and 10 % respectively, and after that the bandgap begins to reduce at a higher rate leading to semiconductor to metal transition at e_z = 39 %, 20 % and 21 % respectively, for α-P, γ-P and δ-P bilayers. However, bandgap reduces monotonically for β-P bilayer thus producing metallization at e_z = 34 % (e_z = 38 % for β-P in rectangular unitcell). In case of hetero-bilayers (except γ-P/δ-P), the bandgap remains constant up to 20 % of strain. For e_z > 20 % the bandgap reduces until metallization occurs at e_z = 39 %. On the other hand, in case of γ-P/δ-P, the applied (NCS) increases the bandgap. The band structures of α-P/β-P at different strain values as a representative case, is shown in Figure S9 of ESI. Although there is no significant change in bandgap of α-P/β-P up to 20 % strain (Figure 7), but the CBM continuously decreases to ~ 20 % and ~ 79 % of its initial values at 13.2 % and 31.6 % of applied strains respectively, while the VBM first increases to ~ 14 % and 22 % of its initial values at 2.6 % and 13.2 % of strains respectively, and then at 21 % of applied strain, the VBM is found to decrease by ~ 2 % where as at 31.6 % of strain it decreases by ~ 56 % of its equilibrium values.

Physical Chemistry Chemical Physics Accepted Manuscript

Also in order to check the experimental feasibility of these NCS induced bandgap variations, we define pressure as the energy per unit area required to reduce the inter layer distance by $\Delta R = (R_0 - R)$, where R and R_0 are the strained and strain-free distances between the bilayers. Therefore, the applied pressure P is given by $(E - E_0)/((\Delta R)*A)$, where E and E_0 are the strained and equilibrium bilayer energies, A is the area of unitcell and ΔR is the change in interlayer distance in moving from equilibrium to the strained configuration. Figure 8 shows the variation of fractional change in bandgap with pressure for the considered homo- and hetero-bilayers.

It is found that applied pressure induces zero bandgap in all the homo- and hetero-bilayers (except γ-P/δ-P) *i.e.* in α-P/α-P (at 7.11 GPa), β-P/β-P (in hexagonal unit cell at 4.77 GPa and in rectangular unit cell at 5.81 GPa (Figure S10 of ESI), γ-P/γ-P (at 2.0 GPa), δ-P/δ-P (at 4.42 GPa), α-P/β-P (at 9.62 GPa), γ-P/β-P (at 8.18 GPa) and δ-P/β-P (at 11.34 GPa) (Figure 8). But in case of α-P/α-P, β-P/β-P, α-P/β-P, γ-P/β-P and δ-P/β-P the zero bandgap value occurs at the interlayer distances that approximately corresponds to the P-P bond length of phosphorene. Thus, the metallization in these cases is a result of covalent bonding between the corresponding layers of the bilayers. In case of γ-P/γ-P and δ-P/δ-P complete semiconductor to metal transition occurs at quite higher interlayer distance (3.0 Å). Applied normal compression strain also produces direct to indirect bandgap transition in α-P as well as in δ-P bilayers at an interlayer distance of 3.1 Å i.e., at $e_z = 18$ % and $e_z = 19$ % respectively, corresponding to a pressure of 2.34 GPa in α-P and 3.63 GPa in δ-P. Among the hetero-bilayers, indirect to direct bandgap transition occurs in case of δ-P/β-P bilayer at $e_z = 35.7$ % or at 5.28 GPa of pressure. The interlayer distance and the value of pressure at which metallization occurs for the considered systems, are depicted in Table 3 and the magnitude of these pressure values indicate their experimental feasibility.

Physical Chemistry Chemical Physics Accepted Manuscript

3.6 Effect of transverse electric field:

Next we examine the effect of external electric field on the electronic properties of the considered homo- and hetero-bilayer systems. The electric field is applied in the range from -1.0 V/Å to +1.0 V/Å in steps of 0.1 V/Å, in a direction perpendicular to the 2D structure. Positive direction of electric field is taken along the positive z direction i.e., from bottom towards the top layer, while negative electric field is applied along negative z-direction. Application of positive and negative electric field shows almost symmetric curve with respect to zero field axes for homo-bilayers (Figure 9(a)) which is attributed to the homogeneity of atoms on the surface of both layers in homo-bilayer system. The application of electric field decreases the bandgap and produces metallization in α-P/α-P, γ-P/γ-P and δ-P/δ-P at ±0.7 V/Å, ±0.5 V/Å and ±0.5 V/Å, respectively .On the other hand, the bandgap gets reduced to ~ 28 % of its initial value at ±1.0 V/Å for β-P/β-P (Figure 9(a)).

Figure 9(b) shows the variation of bandgap in case of hetero-bilayers with positive and negative transverse electric field. The change in bandgap of hetero-bilayers is not same with positive and negative electric field. As a representative case, the electronic band structure and isosurfaces of charge accumulation and charge depletion of α-P/β-P hetero-bilayer in the presence of an applied positive and negative electric field is shown in Figure S11 of ESI. The positive field shows the depletion of charge from the upper surface of heterostructure while negative field induce charge depletion from the lower surface of hetero-bilayer. Both cases lead to the decrease in band gap due to the accumulation of charge within the layers of heterostructures. The application of positive electric field decreases the bandgap linearly until metallization occurs at +0.9 V/Å, whereas with negative electric field, the band structure shows negligible change in bandgap value up to -0.3 V/Å. The bandgap gets reduced on further increase in negative field. The different magnitude of bandgap value with positive and negative field is attributed to the counterbalance of external electric field

Physical Chemistry Chemical Physics Accepted Manuscript

with internal field induced due to the different structural phases and heterogeneity in the arrangements of atoms of each surface of hetero-bilayer system. The complete metallization occurs at +0.9 V/Å for α-P/β-P, at -0.3 V/Å as well as +0.8 V/Å for γ-P/δ-P and at +0.4 V/Å for δ-P/β-P respectively, while γ-P/β-P remains a semiconductor for the considered range of applied electric field with a bandgap value of 0.03 eV at +1.0 V/Å and 0.19 eV at -1.0 V/Å. Among all the bilayers, electric field produces indirect to direct bandgap transition only in δ-P/β-P bilayer at -0.3 V/Å.

4. Summary:

Tuning of electronic properties of homo- and hetero-bilayers of various structural phases of phospherene has been investigated within the DFT framework. Our total energy calculations reveal AB-stacking to be most favorable for α-P bilayer while β-P, γ-P and δ-P bilayers prefer AA-stacking pattern. All the homo-bilayers are found to be semiconducting. The γ-P homo-bilayer structure possess highest UTS values i.e. 6.21 GPa & 4.47 GPa along x and y directions, while for hetero-bilayer the UTS values are calculated in the range of 2.8-6.0 GPa. Both homo- and hetero-bilayers show significant modulation of bandgap on the application of in-plane tensile strain. A transition from semiconductor to metal has been found to occur at a critical value of transverse pressure. The modulation of bandgap strongly depends on polarity of external electric field for hetero-bilayers, due to different structural phases and heterogeneity in the arrangement of atoms on each surface of the bilayer system. The electronic structure engineering by mechanical strain, pressure and transverse electric field in homo- and hetero-bilayers of various structural phases of phosphorene may be useful to fabricate next generation devices based on van der Waals bilayer structures.

Physical Chemistry Chemical Physics Accepted Manuscript

References

1. A. K. Geim, and K. S. Novoselov, *The Rise of Graphene*, Nat. Mater.,2007, **6**, 183.
2. S. Z. Butler, S. M. Hollen, L. Cao, Y. Cui, J. A. Gupta, H. R. Gutiérrez, F. T. Heinz, S. S. Hong, J. Huang, A. F. Ismach, E. Johnston-Halperin, M. Kuno, V. V. Plashnitsa, R. D. Robinson, R. S. Ruoff, S. Salahuddin, J. Shan, L. Shi, M. G. Spencer, M. Terrones , W. Windl and J. E. Goldberger, *Progress, Challenges, and Opportunities in Two-Dimensional Materials Beyond Graphene*, ACS Nano, 2013, *7*, 2898.
3. H. Wang, H. Yuan, S. S. Hong, Y. Li and Y. Cui, *Physical and Chemical Tuning of Two dimensional Transition Metal Dichalcogenides*, Chem. Soc. Rev., 2015, **44**, 2664.
4. Q. H. Wang, K. Kalantar-Zadeh, A. Kis, J. N. Coleman and M. S. Strano, *Electronics and Optoelectronics of Two-dimensional Transition Metal Dichalcogenides*, Nat. Nanotech.,2012, **7**, 699.
5. J. Wu, B. Wang, Y. Wei, R. Yang and M. Dresselhaus, *Mechanics and Tunable Bandgap by Straining in Single-Layer Hexagonal Boron-Nitride,* Materials Research Letters., 2013, **1**, 200.
6. H. Oughaddou , H. Enriquez, M. R. Tchalala, H. Yildirim, A. J. Mayne, A. Bendounan, G. Dujardin, M. A. Ali and Kara, Silicene*, a promising new 2D material,* Progress in Surface Science., 2015, **90**, 46.
7. J.R Brent, N. Savjani, E. Lewis, S. Haigh, D. Lewis, P. O'Brien, *Production of few-layered phosphorene by liquid exfoliation of black phosphorous,* Chem. Comm., 2014, **50,** 13338.
8. S. Das, W. Zhang, M. Demateau, A. Hoffmann, M. Dubey and A. Roelofs, *Tunable Transport Gap in Phosphorene***,** Nano Lett., 2014, **14,** 5733.

Physical Chemistry Chemical Physics Accepted Manuscript

9. L. Li, Y. Yu, G. J. Ye, Q. Ge, X. Ou, H. Wu, D. Feng, X. H. Chen and Y. Zhang, *Black Phosphorus Field-effect Transistors*, Nat. Nanotech., 2014, **9,** 372.

10. F. Xia, H. Wang and Y. Jia, *Rediscovering Black Phosphorus as an Anisotropic Layered Material for Optoelectronics and Electronics*, Nat. Comm., 2014, **5,** 4458.

11. *Y.* Cai, Q. Ke, G. Zhang, Y. P. Feng, V. B. Shenoy, and Y. -W. Zhang*, Giant Phononic Anisotropy and Unusual Anharmonicity of Phosphorene: Interlayer Coupling and Strain Engineering,* Adv. Funct. Mater. 2015, **25**, 2230–2236.

12. Z. Zhu and D. Tománek, *Semiconducting Layered Blue Phosphorus: A Computational Study,* Phys. Rev. Lett., 2014, **112**, 176802.

13. J. Guan, Z. Zhu and D. Tománek, *Phase coexistence and metal insulator transition in few-layer phosphorene: A computational study*, Phys. Rev. Lett., 2014, **113**, 046804.

14. S. E. Boulfelfel, G. Seifert, Y. Grin, and S. Leoni, *Squeezing lone pairs: The A17 to A7 pressure-induced phase transition in black phosphorus*, Phys. Rev. B., 2012, **85**, 014110.

15. M. Wu, H. Fu, L. Zhou, K. Y and X. C. Zeng, *Nine New Phosphorene Polymorphs with Non-Honeycomb Structures: A Much Extended Family*, Nano Lett., 2015, **15**, 3557.

16. L. Kou, C. Chen, and S. C. Smith, *Phosphorene: Fabrication, Properties, and Applications*, J. Phys. Chem. Lett., 2015, **6,** 2794–2805.

17. J. B. Smith, D. Hagaman and H. -F. Ji, *Growth of 2D black phosphorus film from chemical vapor deposition,* Nanotechnology, 2016, **27**, 215602-215609.

18. T. Niu and A. Li, *From two-dimensional materials to heterostructures*, Progress in Surface Science, 2015, **90**, 21.

19. M. Li, C. Chen, Y. Shi and L. Li, *Heterostructures based on two-dimensional layered materials and their potential applications*, Materials Today., 2015, **0**, 1.

Physical Chemistry Chemical Physics Accepted Manuscript

20. P. Rivero, C. M. Horvath, Z. Zhu, J. Guan, D. Tománek, and S. Barraza-Lopez, *Simulated scanning tunneling microscopy images of few-layer phosphorene capped by graphene and hexagonal boron nitride monolayers,* Phys. Rev. B, 2015, **91**, 115413.
21. J. E. Padilha, A. Fazzio, and A. J. R. da Silva, *van der Waals Heterostructure of Phosphorene and Graphene: Tuning the Schottky Barrier and Doping by Electrostatic Gating*, Phys. Rev. Lett*.*, 2015, **114**, 066803.
22. G.-C. Guo, D. Wang, X.-L. Wei, Q. Zhang, H. Liu, W.-M. Lau and L.-M. Liu, *First-Principles Study of Phosphorene and Graphene Heterostructures Anode Materials for Rechargeable Li Batteries,* J. Phys. Chem. Lett*.*, 2015, **6**, 5002.
23. Y. Cai, G. Zhang and Y. –W. Zhang, *Electronic Properties of Phosphorene/Graphene and Phosphorene/Hexagonal Boron Nitride* Heterostructures, J. Phys. Chem. C, 2015, **119,** 13929-13936.
24. Y. Deng, Z. Luo, N. J. Conrad, H. Liu, Y. Gong, S. Najmaei, P. M. Ajayan, J. Lou, X. Xu and P. D. Ye, *Black Phosphorus Monolayer/MoS_2 van der Waals Heterojunction p-n Diode,* ACS Nano*.*, 2014, **8**, 8292.
25. H. Liu, A. T. Neal, Z. Zhu, Z. Luo, X. Xu, D. Tománek and P. D. Ye, *Phosphorene: An Unexplored 2D Semiconductor with a High Hole Mobility,* ACS Nano*.*, 2014, **8**, 4033-4041.
26. K. Gong, L. Zhang, W. Ji, and H. Guo, *Electrical contacts to monolayer black phosphorus: A first-principles investigation*, Phys. Rev. B., 2014, **90,** 125441.
27. X. Peng, Q. Wei and A. Copple, *Strain-engineered direct-indirect bandgap transition and its mechanism in two-dimensional phosphorene*, Phys. Rev. B., 2014, **90**, 085402.

Physical Chemistry Chemical Physics Accepted Manuscript

28. M. Sharma, A. Kumar, P. K. Ahluwalia and R. Pandey, *Strain and electric field induced electronic properties of two-dimensional hybrid bilayers of transition-metal dichalcogenides,* J. Appl. Phys., 2014, **116**, 063711.

29. A. Kumar, H. He, R. Pandey, P. K. Ahluwalia and K. Tankeshwar, *Pressure and electric field-induced metallization in the phase-engineered ZrX_2 (X= S, Se, Te) bilayers,* Phys. Chem. Chem. Phys., 2015, **17**, 19215.

30. R. Fei and L. Yang, Lattice vibrational modes and Raman scattering spectra of strained phosphorene, Appl. Phys. Lett. 2014, **105**, 083120.

31. M. Buscema, D. J. Groenendijk, S. I. Blanter, G. A. Steele, H. S. J. vanderZant, A. Castellanos-Gomez, *Fast and Broadband Photoresponse of Few-Layer Black Phosphorus Field-Effect Transistors,* Nano Lett., 2014, **14,** 3347.

32. S. Liu, N. Huo, S. Gan, Y. Li, Z. Wei, B. Huang, J. Liu, J. Li and H. Chen, *Thickness-dependent Ramanspectra, transport properties and infrared photoresponse in few-layer black phosphorus,* J. Mater. Chem. C., 2015, **3**, 10974.

33. H. Y. Lv, W. J. Lu, D. F. Shao, and Y. P. Sun, *Enhanced thermoelectric performance of phosphorene by strain-induced band convergence*, Phys. Rev. B., 2014, **90**, 085433.

34. R. Fei, A. Faghaninia, R. Soklaski, J.-A. Yan, C. Lo and L. Yang, *Enhanced Thermoelectric Efficiency via Orthogonal Electrical and Thermal Conductances in Phosphorene*, Nano Lett., 2014, **14**, 6393.

35. L. Kou, T. Frauenheim and C. Chen, *Phosphorene as a Superior Gas Sensor: Selective Adsorption and Distinct I–V Response*, J. Phys. Chem. Lett., 2014, **5,** 2675.

36. W. Li, Y. Yang, G. Zhang and Y.-W. Zhang, *Ultrafast and Directional Diffusion of Lithium in Phosphorene for High-Performance Lithium-Ion Battery*, Nano Lett., 2015, **15,** 1691.

Physical Chemistry Chemical Physics Accepted Manuscript

37. J. M. Soler, E. Artacho, J. D. Gale, A. Garcia , J. Junquera, P. Ordejon and D. S. Portal, *The SIESTA method for ab initio order-N Materials Simulation*, J. Phys.: Condens. Matter., 2002, **14,** 2745.

38. N. Troullier and J. L. Martins, *Efficient Pseudopotentials for Plane-Wave Calculations*, Phys. Rev. B, 1991, **43**, 1993.

39. M. Dion, H. Rydberg, E. Schröder, D. C. Langreth, and B. I. Lundqvist, *Van der Waals Density Functional for General Geometries*, Phys. Rev. Lett., 2004, **92**, 246401.

40. J. Dai and X. C. Zeng*, Bilayer Phosphorene: Effect of Stacking Order on Bandgap and Its Potential Applications in Thin-Film Solar Cells,* J. Phys. Chem. Lett., 2014, **5,** 1289.

41. B. Ghosh, S. Nahas, S. Bhowmick, and A. Agarwal, *Electric field induced gap modification in ultrathin blue phosphorus*, Phys. Rev. B., 2015, **91**, 115433.

42. Y. Cai, G. Zhang and Y. –W. Zhang, *Layer-dependent Band Alignment and Work Function of Few-Layer Phosphorene,* Sci. Rep., 2014, **4**, 6677.

43. Q. Liu, X. Zhang, L. B. Abdalla, A. Fazzio and A. Zunger, *Switching a Normal Insulator into a Topological Insulator via Electric Field with Application to Phosphorene,* Nano Lett., 2015, **15**, 1222.

44. Y. Li and X. Chen, *Dirac Fermions in Blue-Phosphorus*, 2D Mater., 2014, **1**, 031002.

45. M. Wu, X. Qian, and J. Li, *Tunable Exciton Funnel Using Moiré Superlattice in Twisted van der Waals Bilayer,* Nano Lett., 2014, **14**, 5350.

46. A. Kumar and P. K. Ahluwalia, *Mechanical strain dependent electronic and dielectric properties of two-dimensional honeycomb structures of* MoS_2 *(X=S, Se, Te),* Physica B., 2013, **419**, 66.

Physical Chemistry Chemical Physics Accepted Manuscript

TABLE 1. Lattice constants (a, b), supercell, number of atoms per unitcell (N), interlayer distance (R), binding energy per atom (E_b) and bandgap (E_g) of the considered homo-bilayers.

Parameter	α-P/α-P		β-P/β-P (hexagonal cell)		γ-P/γ-P		δ-P/δ-P	
Functional	GGA-PBE	vdW	GGA-PBE	vdW	GGA-PBE	vdW	GGA-PBE	vdW
a, b (Å)	3.35 4.47	3.42 4.84	3.32 3.32	3.42 3.42	3.41 5.30	3.41 5.67	5.43 5.38	5.81 5.67
Supercell	1×1	1×1	1×1	1×1	1×1	1×1	1×1	1×1
N	8	8	4	4	8	8	16	16
R (Å)	3.25	3.78	3.49	3.78	2.31	3.73	3.37	3.82
E_b (meV/atom)	31	50	30	57	67	61	34	51
E_g (eV)	0.48	0.92	1.30	1.49	0	0.29	0	0.38

3.35, 4.47

TABLE 2. Lattice constants (a, b), supercell, number of atoms per unitcell (N), interlayer distance (R), binding energy per atom (E_b) and bandgap (E_g) of the considered hetero-bilayers.

Parameter	α-P/β-P		γ-P/δ-P		γ-P/β-P		δ-P/β-P	
Functional	GGA-PBE	vdW	GGA-PBE	vdW	GGA-PBE	vdW	GGA-PBE	vdW
a, b (Å)	3.34 22.55	3.41 24.18	16.47 5.42	17.46 5.67	3.31 5.73	3.41 5.91	16.47 5.42	17.46 5.67
Supercell	5×1(α-P) 4×1(β-P)	5×1(α-P) 4×1(β-P)	5×1(γ-P) 3×1(δ-P)	5×1(γ-P) 3×1(δ-P)	1×1(γ-P) 1×1 (β-P)	1×1(γ-P) 1×1 (β-P)	5×1(β-P) 3×1(δ-P)	5×1(β-P) 3×1(δ-P)
N	36	36	44	44	8	8	44	44
R (Å)	3.50	3.8	3.10	3.7	3.50	3.8	3.50	3.8
E_b (meV/atom)	29	53	36	53	29	55	30	52
E_g (eV)	0.85	1.32	0.13	0.24	0.97	1.02	0.08	0.36

Physical Chemistry Chemical Physics Accepted Manuscript

TABLE 3. Ultimate tensile stress (UTS) S_x and S_y, along x and y directions, corresponding ultimate in-plane biaxial strains (e_x and e_y), ultimate pressure (P_m) and interlayer distance (d_m) at which metallization occurs in the considered bilayer systems.

Parameter	α-P/α-P		β-P/β-P (hexagonal unitcell)		γ-P/γ-P		δ-P/δ-P		α-P/β-P		γ-P/δ-P		γ-P/β-P		δ-P/β-P	
Functional	**GGA-PBE**	**vdW**	**GGA-PBE**	**vdW**	**GGA-PBE**	**vdW**	**GGA-PBE**	**vdW**	**GGA-PBE**	**vdW**	**GGA-PBE**	**vdW**	**GGA-PBE**	**vdW**	**GGA-PBE**	**vdW**
UTS (GPa)																
S_x	6.77	4.79	5.71	4.68	8.27	6.21	4.09	3.00	6.26	5.19	3.84	2.86	6.96	5.98	4.01	2.85
S_y	5.89	4.80	5.71	4.68	6.64	4.47	4.16	3.08	6.52	3.95	3.49	2.82	3.99	3.41	4.92	3.75
e_x (%)	18	16	26	24	30	32	20	20	19	18	23	22	28	26	21	20
e_y (%)	19	22	26	24	18	22	20	18	23	18	17	18	19	18	23	24
P_m (GPa)	2.82	7.11	1.74	4.77	-----	2.0	-----	4.42	7.00	9.62	-----	-----	6.04	8.18	7.73	11.34
d_m (Å)	2.69	2.4	2.50	2.5	-----	3.0	-----	3.0	2.38	2.3	-----	-----	2.3	2.3	2.4	2.3

Physical Chemistry Chemical Physics Accepted Manuscript

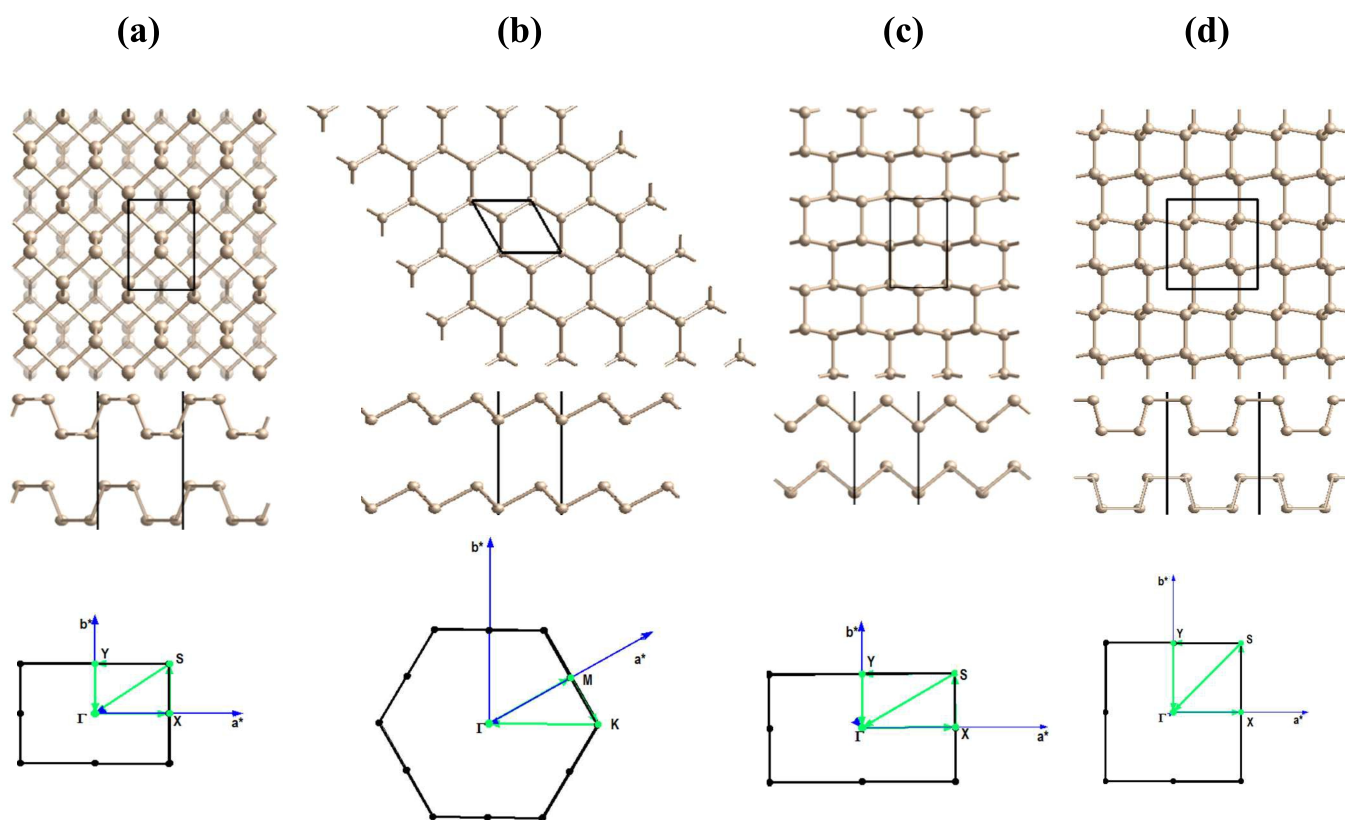

FIGURE 1. Top and side view of homo-bilayers (a) α-P/α-P, (b) β-P/β-P (c) γ-P/γ-P and (d) δ-P/δ-P. (1×1) unit cell is also indicated by solid lines. Light colored atoms in top views represent underneath layer. α-P bilayers stabilized into AB-stacked pattern while β-P, γ-P and δ-P prefers AA-stacking. In the Brillouin zone, a* and b* along the blue lines indicate reciprocal lattice vectors and the green lines show the path chosen for Brillouin zone sampling.

Physical Chemistry Chemical Physics Accepted Manuscript

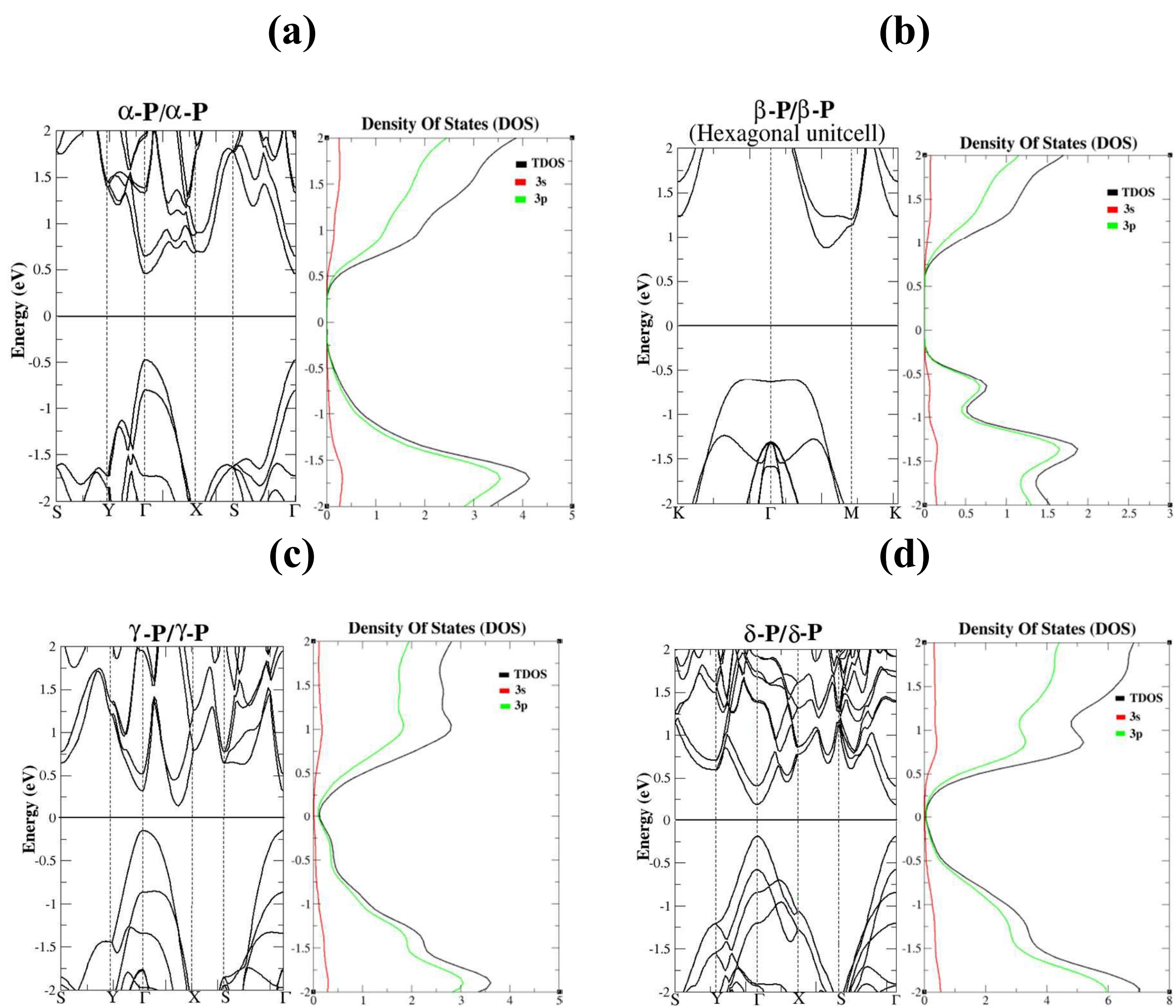

FIGURE 2. The electronic band structure and density of states of the homo-bilayers (a) α-P (b) β-P (c) γ-P and (d) δ-P.

Physical Chemistry Chemical Physics Accepted Manuscript

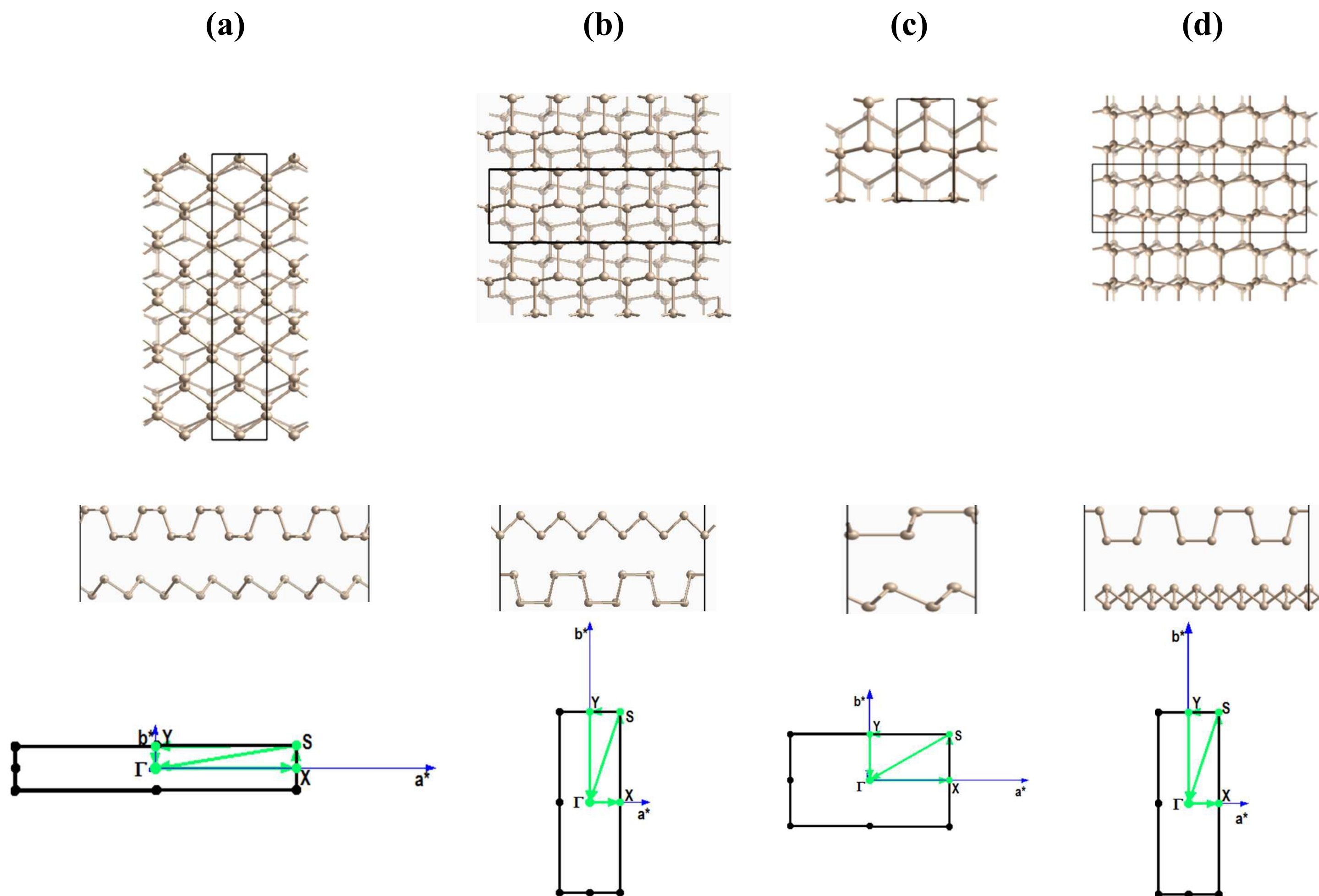

FIGURE 3. Top and side view of the hetero-bilayers (a) α-P/β-P, (b) γ-P/δ-P, (c) γ-P/β-P and (d) δ-P/β-P. Light colored atoms in top view indicate the underneath layer. In the Brillouin zone, a* and b* along the blue lines indicate reciprocal lattice vectors and the green lines show the path chosen for Brillouin zone sampling.

Physical Chemistry Chemical Physics Accepted Manuscript

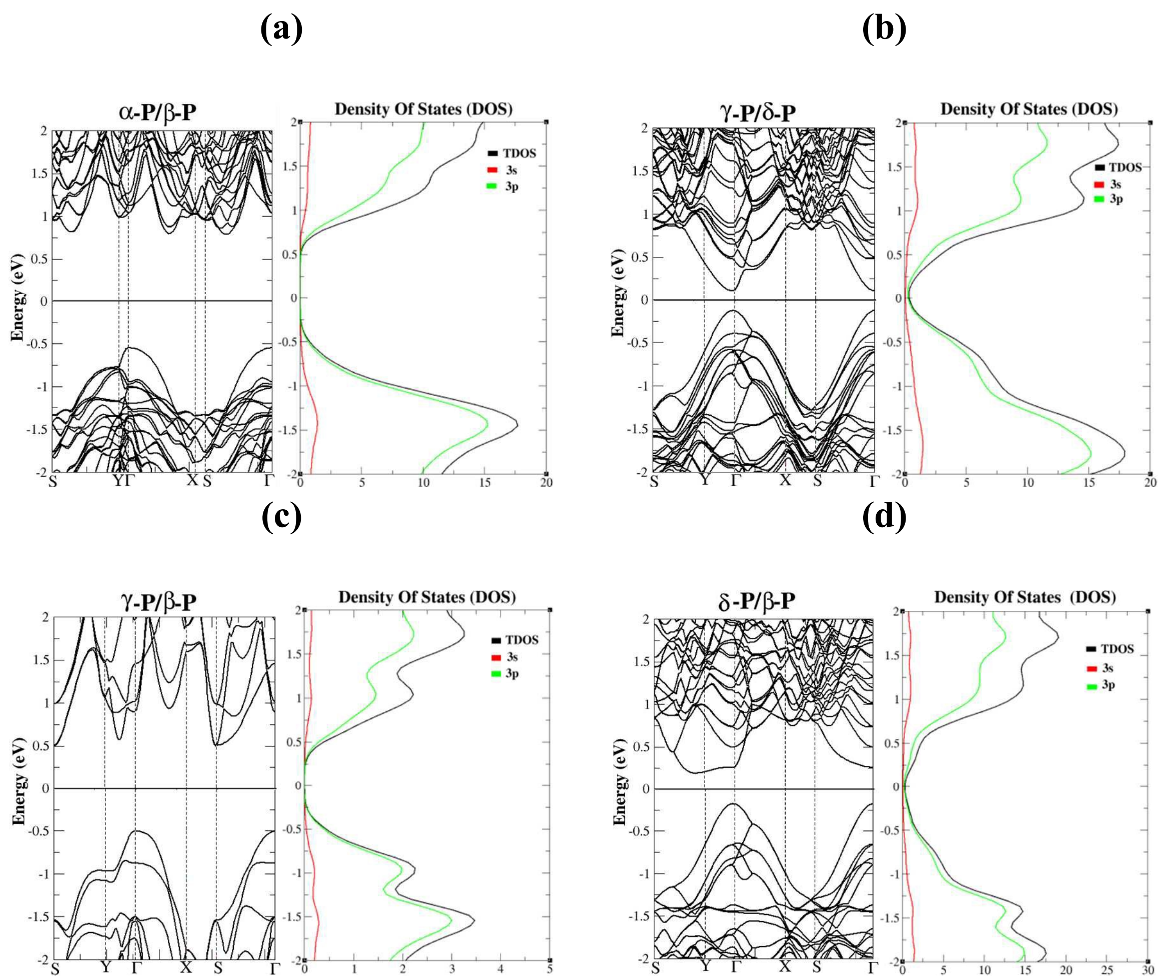

FIGURE 4. The electronic band structure and corresponding total and partial density of states of hetero-bilayers (a) α-P/β-P and (b) γ-P/δ-P, (c) γ-P/β-P and (d) δ-P/β-P.

Physical Chemistry Chemical Physics Accepted Manuscript

Homo-bilayers

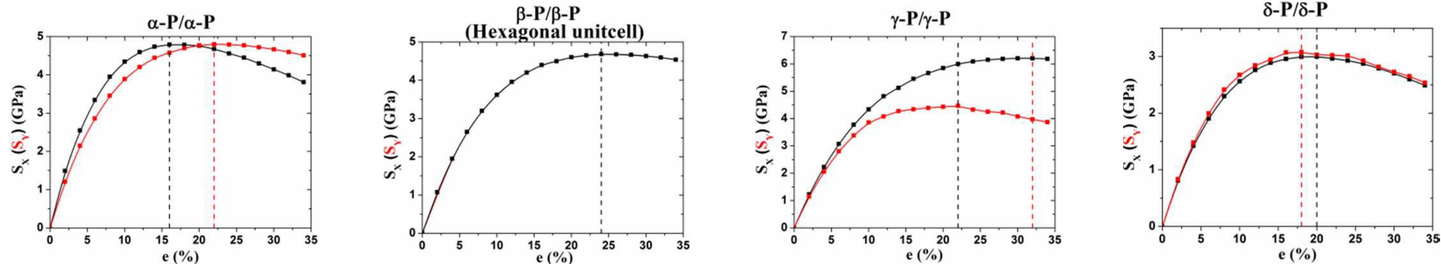

Hetero-bilayers

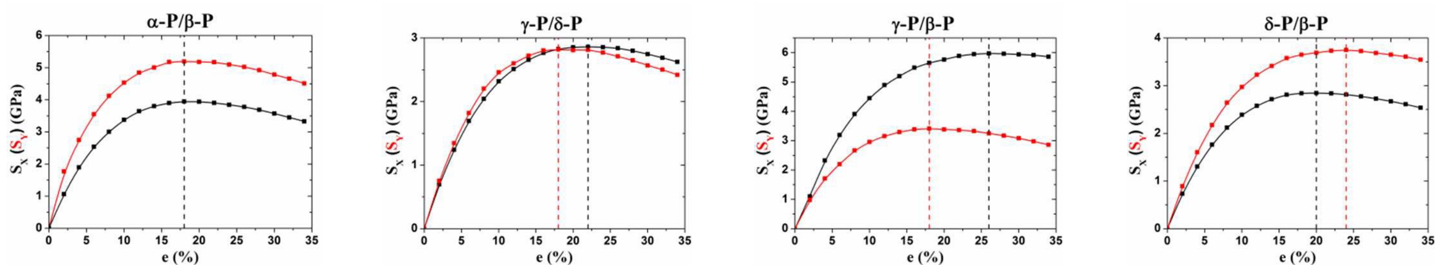

FIGURE 5. The strain-stress curves of the considered homo- and hetero-bilayers of various structural phases of phosphorene. Black/red color shows stress S_x/S_y along x/y direction in response of biaxial strain (e). The vertical lines indicate the ultimate strain value at which slope of strain-stress curve becomes zero.

Physical Chemistry Chemical Physics Accepted Manuscript

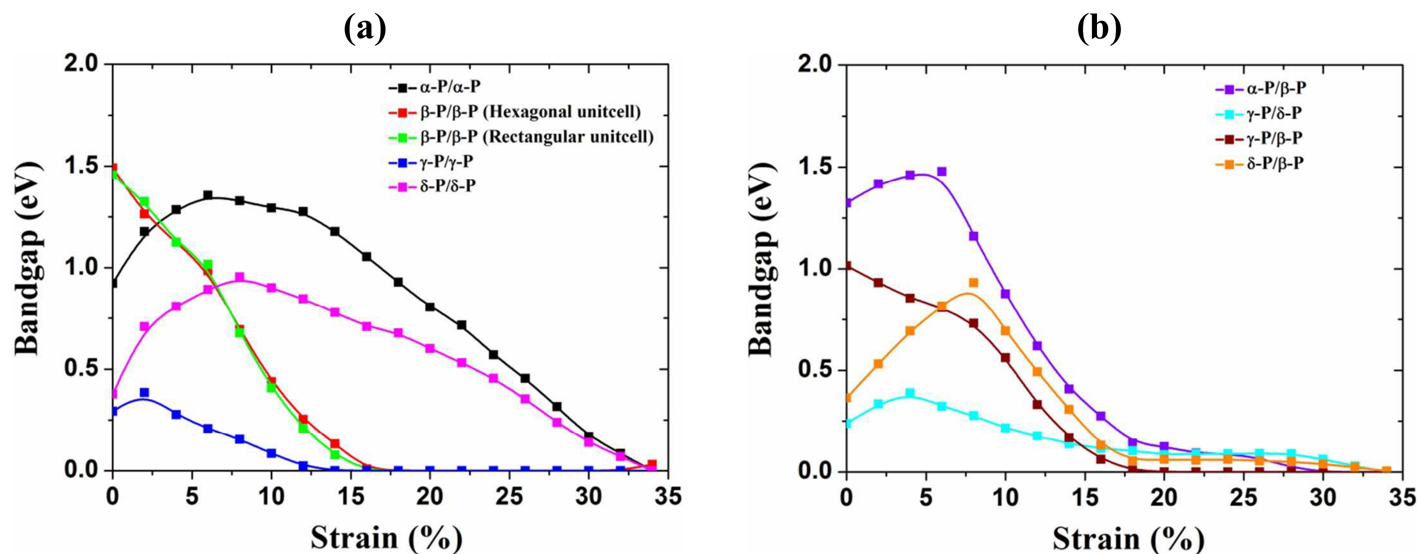

FIGURE 6. The bandgap as a function of biaxial strain in (a) homo-bilayers and (b) hetero-bilayers of various structural phases of phosphorene.

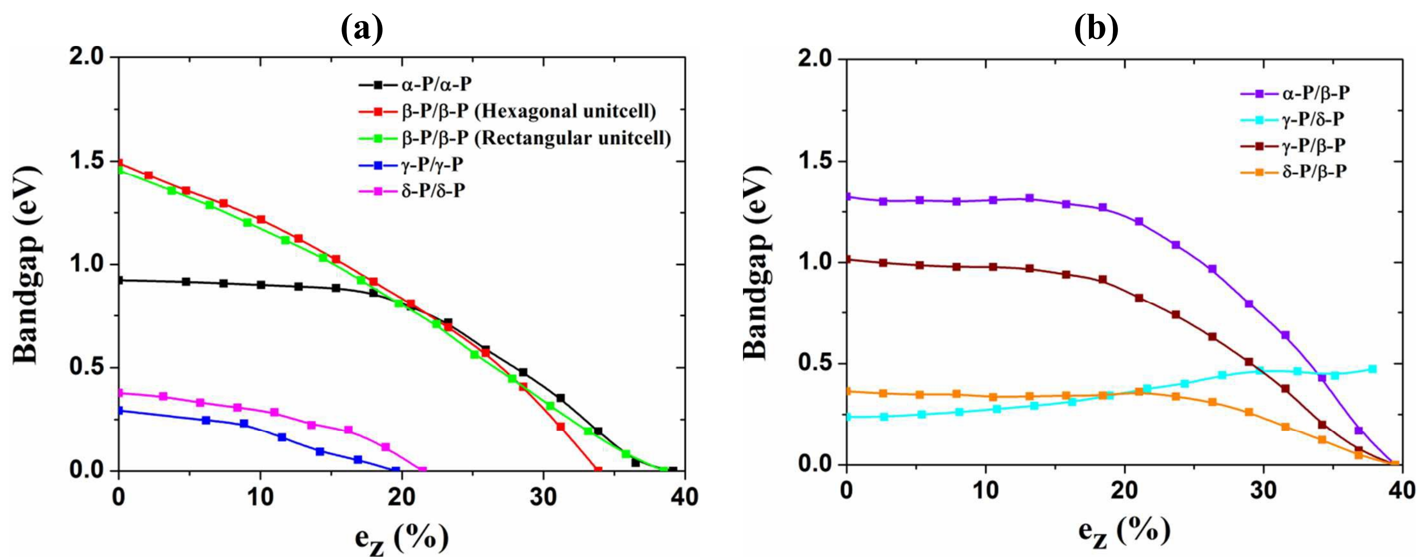

Physical Chemistry Chemical Physics Accepted Manuscript

FIGURE 7. Bandgap Vs. applied normal compression strain (e_z) for (a) homo-bilayers and (b) hetero-bilayers of various structural phases of phosphorene.

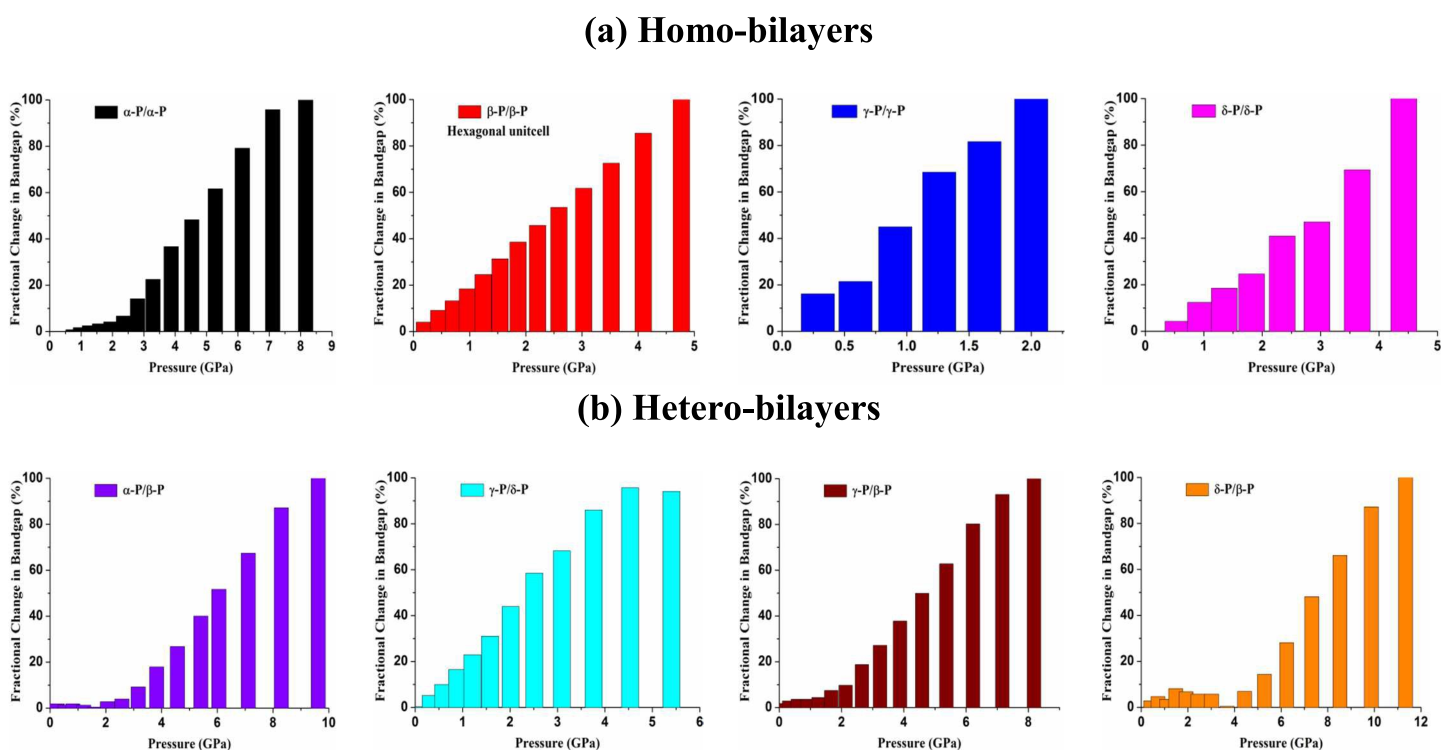

FIGURE 8. The variation of fractional change in bandgap with pressure for (a) homo-bilayers and (b) hetero-bilayers of various structural phases of phosphorene.

Physical Chemistry Chemical Physics Accepted Manuscript

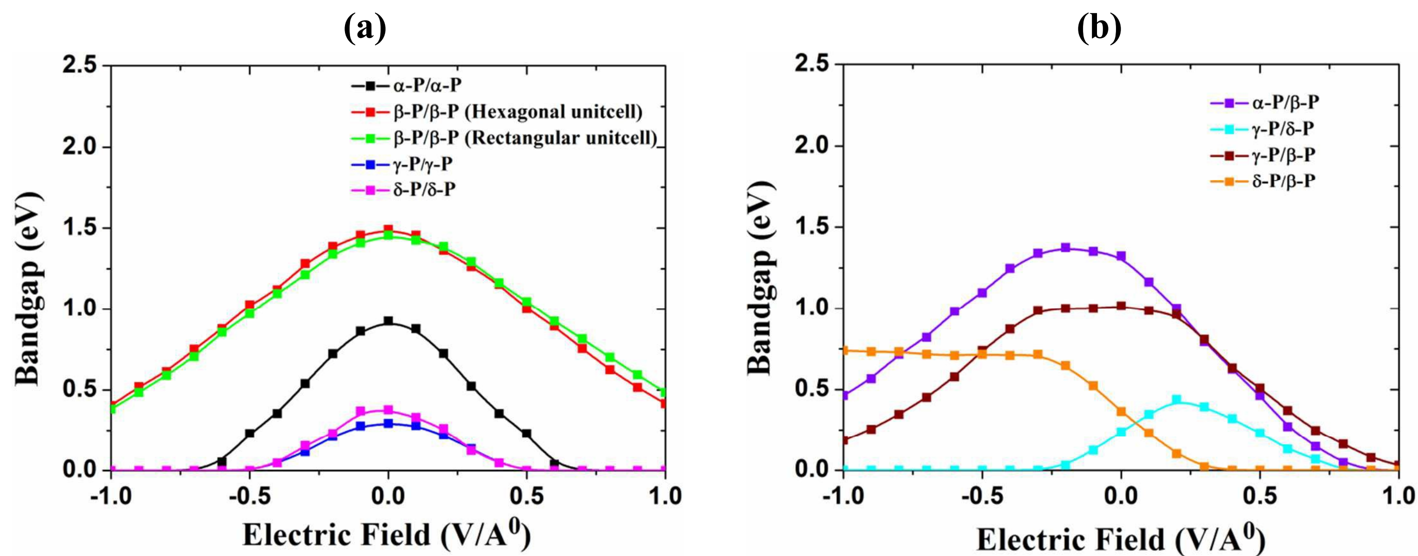

FIGURE 9. The bandgap variation with electric field for (a) homo-bilayers and (b) hetero-bilayers of various structural phases of phosphorene.

Physical Chemistry Chemical Physics Accepted Manuscript